

CIRCULATION COPY
SUBJECT TO RECALL
TWO WEEKS

UCRL-90551
PREPRINT

The $^{152,154}\text{Eu} (t, \alpha)$ Reactions:
Studies of the $11/2^-[505]$ Bands in ^{151}Sm and ^{153}Sm

H.E. Martz
R.G. Lanier
G.L. Struble
L.G. Mann
R.K. Sheline
W. Stöffl

This paper was submitted to
Nuclear Physics A

March 1984

Lawrence
Livermore
National
Laboratory

This is a preprint of a paper intended for publication in a journal or proceedings. Since changes may be made before publication, this preprint is made available with the understanding that it will not be cited or reproduced without the permission of the author.

DISCLAIMER

This document was prepared as an account of work sponsored by an agency of the United States Government. Neither the United States Government nor the University of California nor any of their employees, makes any warranty, express or implied, or assumes any legal liability or responsibility for the accuracy, completeness, or usefulness of any information, apparatus, product, or process disclosed, or represents that its use would not infringe privately owned rights. Reference herein to any specific commercial products, process, or service by trade name, trademark, manufacturer, or otherwise, does not necessarily constitute or imply its endorsement, recommendation, or favoring by the United States Government or the University of California. The views and opinions of authors expressed herein do not necessarily state or reflect those of the United States Government or the University of California, and shall not be used for advertising or product endorsement purposes.

The $^{152,154}\text{Eu}(t,\alpha)$ Reactions:
Studies* of the $11/2[505]$ Bands in ^{151}Sm and ^{153}Sm

H. E. Martz,[†] R. G. Lanier, G. L. Struble
L. G. Mann, R. K. Shelton[†] and W. Stöffl

Nuclear Chemistry Division
Lawrence Livermore National Laboratory
Livermore, CA 94550

*Work taken in part from a thesis submitted by H. E. Martz to the Florida State University for the requirements of an M.S. Degree.

[†]Permanent address: Chemistry Department, Florida State University,
Tallahassee, FL 32306.

ABSTRACT

Radioactive targets of ^{152}Eu (13 y) and ^{154}Eu (8.5 y) have been used to study the $^{152,154}\text{Eu}(t,\alpha)^{151,153}\text{Sm}$ reactions at an incident triton energy of 16 MeV. In these studies, we have identified the band head and three excited rotational states of the $11/2[505]$ neutron orbital in both the $^{151,153}\text{Sm}$ nuclei. The angular distributions and relative intensities for states in this band in both $^{151,153}\text{Sm}$ are reproduced reasonably well by using DWBA calculations and by assuming strongly deformed single-particle wave functions. We have used our results and the results of other studies to determine the equilibrium prolate shapes of both $^{151,153}\text{Sm}$ when the odd neutron quasiparticle occupies the $11/2[505]$ orbital. We estimate $\beta_2 \sim 0.26$ for ^{151}Sm and $\beta_2 \sim 0.3$ for ^{153}Sm .

NUCLEAR REACTIONS: Radioactive ^{152}Eu (13 y) and ^{154}Eu (8.5 y) targets; $^{152,154}\text{Eu}(t,\alpha)^{151,153}\text{Sm}$, $E_t = 16$ MeV; measured Q-Value, $\sigma(\theta)$ with Q3D spectrograph; deduced ^{151}Sm and ^{153}Sm level energies, I^π and Nilsson configurations. Anomalous intensities: Deformation, β_2 , inferred for $11/2[505]$ neutron orbitals.

I. INTRODUCTION

The transition from a spherical to a deformed shape in light rare-earth nuclei is rather abrupt. This contrasts with the somewhat more gradual shape transitions near $Z \sim 76$ and for heavier nuclei in the actinide region. The abrupt rare-earth transition has been interpreted¹⁻⁹ as a consequence of combining the effects of the steeply upsloping $11/2[505]$ neutron orbital with those of the down-sloping orbitals above the $N = 82$ shell. Strongly deformed structures are believed to be caused in some nuclei near the $N \sim 89$ transition region when an unpaired neutron blocks the $11/2[505]$ orbital. This idea has been tested by microscopic Hartree-Bogoliubov calculations¹⁰ to study shape stability in ^{151}Gd . These calculations yield a stable and strongly deformed nuclear structure whenever the $11/2[505]$ orbital is blocked.

The existence of a rotational band associated with the $11/2[505]$ neutron orbital has recently been suggested by experimental γ -ray work in several $N \sim 89$ transitional nuclei. Particular examples include $^{151,153,155}\text{Gd}$ [2,11,12] and $^{149,151,153}\text{Sm}$ [13,14,15]. In these nuclei, the basis for identifying the $11/2[505]$ band members has been rotational-energy and half-life systematics. Furthermore, the population of states associated with the $11/2[505]$ band is observed in $(^3\text{He}, \alpha)$ reaction studies.¹⁶⁻¹⁹ This result is consistent with the expected high-spin and single neutron-hole character of the $11/2[505]$ orbital.

In the present work, the transitional nuclei ^{151}Sm ($N = 89$) and ^{153}Sm ($N = 91$) were studied by the (t, α) reaction on specially fabricated radioactive targets of ^{152}Eu (13 y) and ^{154}Eu (8.5 y). Since the ground-state

configuration of both targets is $\{\pi 5/2[413]; \nu 11/2[505]\}_{K=3^-}$, we expect that all states populated with significant intensity by proton pickup will have an unpaired neutron in the $11/2[505]$ orbital. We have used the results from the present experiment and the results of other studies^{5,6} to estimate the equilibrium prolate shapes of both $^{151,153}\text{Sm}$ when the odd neutron occupies the $11/2[505]$ orbital.

II. EXPERIMENTAL

The (t, α) experiments were performed at the Los Alamos National Laboratory (LANL) P-9 Tandem van de Graaff accelerator facility using a beam of 16 MeV tritons ($\sim 0.2 \mu\text{A}$). The outgoing alpha particles were momentum analyzed with a quadrupole-triple-dipole (Q3D) magnetic spectrograph and were detected with a 1-m long helical proportional counter mounted along the focal plane of the spectrograph. The enriched radioactive ^{152}Eu ($\sim 92\%$) and ^{154}Eu ($\sim 87\%$) targets were $\sim 20 \mu\text{g}/\text{cm}^2$ thick and were supported on $\sim 50 \mu\text{g}/\text{cm}^2$ carbon foils. Although the targets were prepared with an isotopic purity of $\sim 99.9\%$, the enrichment level had declined to $\sim 90\%$ before the present (t, α) experiments were done. This was caused by the accumulation of isobaric decay products during an interval of ~ 19 months between the time when the targets were made and when they were subsequently used for these experiments. Based on the branching ratios of the various β decays, we expect a contamination mixture of ^{152}Gd ($\sim 2\%$) and ^{152}Sm ($\sim 6\%$) in the ^{152}Eu target and virtually only the single contaminant ^{154}Gd ($\sim 13\%$) in the ^{154}Eu target. The threshold for the appearance of (t, α) peaks due to these contaminants (expressed as relative excitation energy) occurs at $\sim 1.7 \text{ MeV}$ (^{152}Gd) in the ^{152}Eu (t, α) spectrum and

at ~ 1.2 MeV (^{154}Gd) in the $^{154}\text{Eu}(t, \alpha)$ spectrum. Details of the target preparations²⁰ and of the experimental arrangement²¹ have been described previously.

Representative spectra from the $^{152}\text{Eu}(t, \alpha)$ and $^{154}\text{Eu}(t, \alpha)$ reactions are shown in Figs. 1 and 2. Each spectrum shown is a computer reconstruction from the original data such that (a) the ordinate scale is properly normalized to the differential cross section and (b) the abscissa is linear in energy. Moreover, to facilitate comparison of various features in the data, the spectra have been shifted so that the centroid of any ground-state population occurs at the same channel position. The data were calibrated by measuring the states observed in the (t, α) reactions on targets of ^{191}Ir and ^{193}Ir . Energy values^{22,23} of the strongly populated states²⁴ from the calibration targets were taken from published compilations. The energy resolution observed for well-resolved and isolated peaks was ~ 20 keV. A spectral fitting program²⁵ that uses a Gaussian line shape was used to extract the positions of the observed particle groups. At excitation energies above ~ 1.5 MeV where the level density is high and the spectra exhibit numerous peaks, it is likely that the particle groups identified by the fitting procedure are unresolved multiplets of individual states with large cross sections. We have determined the integrated strength for several regions of the spectra at high excitation energy and comment on these results in the Discussion (Section III).

The ground states of ^{151}Sm and ^{153}Sm were not populated in our reaction studies. We determined that the Q_1 -value of the lowest energy α -particle group is 13943 ± 15 keV for ^{151}Sm and 13247 ± 11 keV for ^{153}Sm . The energy error for each value is due to a combination of the uncertainty in the

tabulated²⁵ Q_0 value and of the uncertainty in the target thickness and the resultant energy-loss correction for the calibration reaction. To establish an excitation energy scale, we used the ground state Q_0 -values obtained from compilations²⁶ (^{151}Sm , $Q_0 = 14214.5 \pm 0.7$ keV; ^{153}Sm , $Q_0 = 13346.5 \pm 2.2$ keV) and our measured Q_1 -values. Combining these data, we obtained 272 ± 15 keV for the lowest state observed in ^{151}Sm and 100 ± 11 keV for the corresponding state observed in ^{153}Sm . A summary of the α -particle groups observed in both nuclei is given in Tables 1 and 2. The groups are numbered to correspond to the peak labels noted in Figs. 1 and 2, respectively. The energies quoted are obtained from a renormalization of our measured scale to a more precise reference determined from the data obtained by in-beam γ -ray studies.^{14,15} These γ -ray measurements establish the excitation energy of the $11/2[505]$ band head in both Sm nuclei (^{151}Sm , 261.1 keV; ^{153}Sm , 98.4 keV) with good accuracy. Thus, for each set of reaction data, we have adjusted our energy scale (see Section III) so that peak number 1 corresponds to the energy of the $11/2[505]$ band head.

Angular distributions were measured at selected angles between 12.5° and 50° for both reactions. Because of instrumental problems, the data from some of the exposures involving the $^{152}\text{Eu}(t, \alpha)$ reaction were lost, and these angular distributions are less complete. Moreover, the presence of light impurities in the target as well as generally poor statistics precluded us from obtaining angular distributions for the low-intensity but reasonably well-resolved peaks around $E_{\text{ex}} \sim 1.2$ MeV in both spectra. Angular distribution information was not extracted for the higher energy peak groups.

The reaction yield data measured in the spectrograph were corrected for dead-time losses, and the data recorded at different angles were normalized to the number of elastic scattering events counted in a solid-state detector placed at 30° with respect to the beam. The absolute cross sections were derived by normalizing the monitor elastic yields to optical model calculations (see Table 3 for parameters) of the elastic-scattering cross section and by using the known ratio of the monitor and spectrograph solid angles.²⁷

A distorted-wave Born-approximation (DWBA) analysis of the measured angular distributions was performed using the code DWUCK²⁸ and the optical model parameters²⁹ shown in Table 3. In our calculations the finite range and nonlocality parameters were taken as zero for both (t, α) reactions. Experimental angular distributions for the lowest lying states observed in the (t, α) studies are shown in Figs. 3 and 4. The solid lines are the results of DWBA calculations (see Section III).

III. RESULTS AND DISCUSSION

The transition from a spherical to a deformed ground-state shape in light rare-earth nuclei is abrupt. This is emphasized by the plot in Fig. 5 of the binding energy³⁰ of the last two neutrons, S_{2n} , as a function of the mass number A. This plot shows a clear discontinuity at neutron number N ~89. Simple mass calculations show that there is an increase in binding energy of ~1 MeV in crossing the two-neutron gap from N = 88-90 in even-even nuclei in this transition region. This stabilization is interpreted as a change in the shape of the nuclear ground state from spherical to spheroidal.

The reaction yield data measured in the spectrograph were corrected for dead-time losses, and the data recorded at different angles were normalized to the number of elastic scattering events counted in a solid-state detector placed at 30° with respect to the beam. The absolute cross sections were derived by normalizing the monitor elastic yields to optical model calculations (see Table 3 for parameters) of the elastic-scattering cross section and by using the known ratio of the monitor and spectrograph solid angles.²⁷

A distorted-wave Born-approximation (DWBA) analysis of the measured angular distributions was performed using the code DWUCK²⁸ and the optical model parameters²⁹ shown in Table 3. In our calculations the finite range and nonlocality parameters were taken as zero for both (t, α) reactions. Experimental angular distributions for the lowest lying states observed in the (t, α) studies are shown in Figs. 3 and 4. The solid lines are the results of DWBA calculations (see Section III).

III. RESULTS AND DISCUSSION

The transition from a spherical to a deformed ground-state shape in light rare-earth nuclei is abrupt. This is emphasized by the plot in Fig. 5 of the binding energy³⁰ of the last two neutrons, S_{2n} , as a function of the mass number A . This plot shows a clear discontinuity at neutron number $N \sim 89$. Simple mass calculations show that there is an increase in binding energy of ~ 1 MeV in crossing the two-neutron gap from $N = 88-90$ in even-even nuclei in this transition region. This stabilization is interpreted as a change in the shape of the nuclear ground state from spherical to spheroidal.

The (t,α) spectra from the two reactions are very similar in gross appearance (see Figs. 1 and 2) and are characterized by a small number of states with $E_{ex} < 1$ MeV and a high density of states populated well above 1 MeV. A cursory analysis of the four lowest lying states in each spectrum shows that they qualitatively exhibit the intensity pattern expected for a well-deformed $11/2[505]$ rotational band and would easily be populated by pickup of the $5/2[413]$ valence proton from the odd-odd target. We remark on a similar and contrasting comparison⁷ observed in (d,t) and (d,p) studies with the ^{152}Eu target. Pickup of the valence neutron from ^{152}Eu yields a spectrum that shows considerable fragmentation of the $5/2[413]$ rotational strength in ^{151}Eu . By contrast, the (d,p) stripping spectrum shows a very well-developed $5/2[413]$ rotational structure in ^{153}Eu .

As we have noted, the first four particle groups observed in each (t,α) spectrum are assigned as rotational states belonging to the $11/2[505]$ band. Our measured band head energies agree within experimental error with results from in-beam measurements.^{14,15} Moreover, by adjusting our energy scale to the in-beam results, we get reasonable agreement with the rotational energies up to $I^\pi = 17/2^-$ (Tables 1 and 2). We note, however, that our rotational energies for ^{151}Sm appear systematically higher — although still within our error limits — than the in-beam results. We have been unable to determine the source of this systematic effect or if it is significant. In Table 4, we compare the rotational parameters for ^{151}Sm and ^{153}Sm using our measured energy differences. The smooth monotonically decreasing trend is consistent with the general rotational stability and unperturbed structure exhibited by the $11/2[505]$ band in other nuclei in this mass region.

The measured angular distributions were compared with theoretical results obtained by combining DWBA calculations with spectroscopic factors appropriate for pickup from a deformed and non-zero spin target. In particular, the theoretical differential cross section for populating a state in the final nucleus by a (t, α) reaction is given by:²⁸

$$\frac{d\sigma}{d\Omega}(\theta) = N \frac{2I_B+1}{2I_A+1} \sum_j A_{lsj}^2 \frac{\phi_{jl}^{DWBA}(\theta)}{2j+1} \quad (1)$$

where N is the DWBA normalization factor, I_A and I_B are the total spin of the initial and final nuclear states, respectively, $\phi_{jl}^{DWBA}(\theta)$ is the intrinsic single-particle cross section in $\mu\text{b/sr}$ calculated by the program²⁸ DWUCK, l is the angular momentum transfer of the particle with total spin j , and A_{lsj} is the overlap integral that contains the nuclear structure information. The various forms of A_{lsj} appropriate for populating one- and three-quasiparticle final states are given in Table 5. Because the spin of the target is non-zero, Eq. 1 does not, in general, reduce to a simple form involving only one partial wave. Thus, the angular distributions observed are complicated mixtures of various l components.

The parameters used for the optical potential²⁹ are given in Table 3, and we used an overall normalization factor²⁸ of $N = 23$ for the DWBA results. We took $U^2 = 0.5$ for the occupation probability of the active orbital, $\{5/2[413]\}$, and used the Nilsson coefficients, W_{lj} , for $\beta_2 = 0.3$ from the tabulation of Chi.³¹ A comparison of the calculated and experimental angular distributions for the $11/2[505]$ bands is shown in Figs. 3 and 4. In Fig. 6,

we compare the experimental and calculated intensity patterns observed at 30° . The comparisons show generally good agreement between experiment and theory in both Sm nuclei. This agreement, as well as the generally well-behaved rotational parameters exhibited by both bands, is strong corroboration for the essentially strongly deformed character of these states.

We have also calculated the angle-integrated cross sections of the two most strongly populated levels in both $11/2[505]$ bands. A comparison of these results is given in Table 6. Although the errors are large, there appears to be a significant difference ($\sim 20\%$) in the total intensities recorded from both targets. The theoretical values (Table 6) were calculated by assuming identical deformations for the residual nuclei ($\beta_2 = 0.3$) and the intensities of similar states are predicted to be approximately the same ($\pm 2\%$).

We speculate that any difference in the charged-particle pickup population of essentially identical states in different nuclei results from a deformation difference between the target and the residual nucleus. In the present case, the cross section data suggest that, if the deformed cores of ^{154}Eu and ^{153}Sm are the same, then those of ^{152}Eu and ^{151}Sm differ significantly. The deformations ($\beta = \beta_2$) of the targets have been determined ($\pm 10-20\%$) and are 0.28 and 0.30 for ^{152}Eu and ^{154}Eu , respectively.^{5,6} We can estimate the ratios of these deformations by using the relationship $\frac{1}{2} \sim A^{5/3} \beta^2$, which follows from assuming that the nucleus is an irrotational fluid with constant density.³² For the Eu nuclei, we obtain $(\beta_{152}/\beta_{154})_{\text{exp}} \sim 0.93$, which agrees reasonably well with the value $(\beta_{152}/\beta_{154})_{\text{irrot}} \sim 0.96$. To obtain the latter result, we have used the moments of inertia, $\frac{1}{2}$, derived from the energy spacing^{5,6} between the band head and first-excited rotational state. Here, as

in the Sm nuclei, we are considering only bands that involve the $11/2[505]$ neutron orbital. We note that although the irrotational fluid prescription neglects odd-particle effects, the derived deformation ratios may be expected to be reliable for identical configurations because such odd-particle effects should approximately cancel out. To a good approximation $\sim \pm 3\%$, these assumptions seem to be true for the Eu target nuclei. If we apply these same assumptions to the Sm nuclei and evaluate β from the data in Table 4, we obtain $(\beta_{151}/\beta_{153})_{\text{irrot}} \sim 0.90$. Therefore, by dividing the two ratios we obtain the following relationship between the deformations of the target and residual nuclei.

$$(\beta_{151}/\beta_{152})_{\text{irrot}} \sim 0.94 \cdot (\beta_{153}/\beta_{154})_{\text{irrot}}.$$

Although the experimental ^{153}Sm cross sections are larger than what we predict from model calculations, we assume that the measured values represent approximately the full strength, and this suggests⁶ $\beta_{153} \sim \beta_{154} \sim 0.3$. With this assumption and using⁵ $\beta_{152} \sim 0.28$, we obtain $\beta_{151} \sim 0.94 \cdot \beta_{152} \sim 0.26$. Although these calculations are crude and some of the assumptions are not well established, they are qualitatively consistent with our cross section comparison. Detailed structure and reaction calculations would be required to relate quantitatively the difference in deformation between the target and residual nuclei ($\sim 7\%$) to the reduction in the charged-particle cross sections ($\sim 20\%$).

In studies of the $^{152}\text{Eu}(d,t)$ reaction,⁷ we observed a significant fragmentation of the expected $5/2[413]$ rotational strength in ^{151}Eu . The small difference that we observe between the intensities of the $11/2[505]$ band

in $^{151,153}\text{Sm}$ suggests that a similar, but certainly less severe, fragmentation is occurring in ^{151}Sm . That is, the 20% intensity deficiency in the $11/2[505]$ band in ^{151}Sm may be distributed over other states that involve the odd particle coupled to various 0^+ core states. With reference to Fig. 1, we note a reasonably well-resolved group of states at low excitation energy (~ 1.2 MeV) relative to the $11/2[505]$ band. We find that the integrated intensity of these additional states would account for the 20% intensity deficiency estimated between the $11/2[505]$ bands in the Sm nuclei. From theory and by analogy with what was observed⁷ in ^{151}Eu , we expect these states to have the same spins, parities, and angular distributions as the states observed in the $11/2[505]$ band. Unfortunately, because of both poor statistics at other angles and interferences from light impurities, we were unable to extract reliable angular distribution data for these states. It would be interesting to investigate in future experiments the nature of these states more thoroughly.

We have noted that in the (t,α) experiments the rotational states of the $11/2[505]$ bands have been populated up to $I^\pi = 17/2^-$. This is interesting because in the first-order application of the Nilsson model and by assuming a one-step reaction mechanism, the population of spins $>15/2^-$ are not allowed. Admixtures from higher oscillator shells in states of the target or in the residual nucleus could be responsible for this anomalous result. However, candidate orbitals for such $\Delta N = 2$ mixing effects are separated by several MeV and because the interaction³³ matrix element should be typically ~ 100 keV, such effects must be virtually absent. It seems more probable that two-step process³⁴ in the (t,α) reaction mechanism are responsible for populating the $17/2^-$ states.

The states with $E_{ex} > 1$ MeV observed in the (t, α) studies are most probably strongly deformed ($\beta_2 \sim 0.3$) and are essentially one-proton holes coupled to the $\{\pi 5/2[413]; \nu 11/2[505]\}_{K=3^-}$ ground state configuration of the target. The strongest support for this hypothesis would be the identification of individual rotational bands in this energy region. Unfortunately, meaningful configuration assignments for these higher energy peaks are not possible because there is insufficient energy resolution in the experiments and because a number of different partial waves can contribute to the intensities of the observed states. This latter complication is a result of the non-zero spin of the target and is difficult to circumvent without sensitive angular distribution data.

However, we note some of the interesting features observed among the multitude of states populated above 1.2 MeV in both ^{151}Sm and ^{153}Sm . We expect that in both nuclei the observed spectrum is caused primarily by populating deformed three-quasiparticle states that involve an odd-proton hole coupled to the $\{\pi 5/2[413]; \nu 11/2[505]\}_{K=3^-}$ target state. A comparison of both spectra between ~ 1.2 and 2.3 MeV shows a considerable difference in the distribution of the (t, α) strength. In particular, in ^{151}Sm the strength appears to be concentrated in a relatively narrow band between ~ 1.7 and 2.3 MeV. In ^{153}Sm , the distribution appears to be much wider. Moreover, comparing the integrated intensity in both spectra between ~ 1.2 and 2.3 MeV (see the regions of spectra in Figs. 1 and 2 labeled A) shows that $I(^{151}\text{Sm}) \sim 0.6 \cdot I(^{153}\text{Sm})$. This large difference seems to have two possible explanations. The first is that there has been a significant shift in the deformed single particle orbitals and $\sim 40\%$ of the (t, α) strength seen in

^{153}Sm lies at higher energies in ^{151}Sm . The intensity discrepancy may also occur because in ^{151}Sm many of the specific three-quasiparticle configurations populated in our (t, α) experiments are not strongly deformed. Thus, intensity would be distributed over many states and over a wide range of energy. We have noted in previous studies a strong correlation between deformation and the blocking of the $11/2[505]$ neutron orbital. This observation argues strongly that all three-quasiparticle states involving a proton hole coupled to the $\{\pi 5/2[413]; \nu 11/2[505]\}_{K=3^-}$ configuration are strongly deformed. However, because the strongest evidence for correlating strong deformation with blocking the $11/2[505]$ orbital arises from data at low energies, the large difference in the gross spectral features for $E_{\text{ex}} > 1.2$ MeV in both ^{151}Sm and ^{153}Sm may suggest that such a simple extrapolation to higher energies and to complex states may not be valid.

Another feature of the high excitation energy data is the presence of a narrow, intense structure (see the portion of the spectra labeled B in Figs. 1 and 2) that appears very similar in both ^{151}Sm and ^{153}Sm . The lowest energy member occurs at ~ 2.68 MeV in ^{151}Sm and at ~ 2.47 MeV in ^{153}Sm . The structure is particularly interesting because it occurs at very nearly the same energy (~ 160 keV) relative to the $11/2[505]$ band head and has approximately the same strength. We have no explanation for this unusual feature. We have determined that the structure cannot be due to protons, deuterons or tritons that might have "leaked through" the gating electronics. Finally, we have checked for possible (t, α) peaks from various known target impurities and we were unable to find any reasonable correlations.

IV. SUMMARY

We have investigated the structure of ^{151}Sm and ^{153}Sm by using the (t, α) reaction and radioactive targets of ^{152}Eu (13 y) and ^{154}Eu (8.5 y). Below ~ 1 MeV of excitation, we observe from both targets the population of members of only the $11/2[505]$ band. The observed cross sections and angular distributions are reproduced reasonably well by assuming that the target and residual nuclei are equally and strongly deformed. A closer look at the reaction cross sections suggests, however, that the $11/2[505]$ band in ^{151}Sm is populated $\sim 20\%$ less than the population in ^{153}Sm . We show that this intensity reduction is plausible and qualitatively in accord with a small relative deformation difference between the ^{152}Eu target and ^{151}Sm residual nuclei. Finally, we remark on several interesting features of the spectra above 1 MeV. In particular, we observe an intense, narrow structure at ~ 2.5 MeV in both spectra.

ACKNOWLEDGEMENTS

We wish to thank Dr. T. Udagawa for providing us with various analytic forms of the spectroscopic factors used in the cross section calculations. We also thank the staff of the LLNL isotope separator facility and the LANL Tandem van de Graaff facility for their important contributions to the (t, α) experiments.

This work was performed under the auspices of the U.S. Department of Energy by the Lawrence Livermore National Laboratory under contract number W-7405-ENG-48, and under contract PHY79-08395 between the National Science Foundation and the Florida State University.

REFERENCES

1. B. R. Mottelson and S. G. Nilsson, Phys. Rev. 99, 1615 (1955).
2. H. J. Smith, D. G. Burke, M. W. Johns, G. Løvholden, and J. C. Waddington, Phys. Rev. Lett. 31, 944 (1973); P. Kleinheinz, R. K. Sheline, M. R. Maier, R. M. Diamond, and F. Stephens, Phys. Rev. Lett. 32, 68 (1974).
3. G. L. Struble, I. C. Oelrich, J. B. Carlson, L. G. Mann, and R. G. Lanier, Phys. Rev. Lett. 39, 533 (1977).
4. R. G. Lanier, G. L. Struble, L. G. Mann, I. D. Proctor, and D. W. Heikkinen, Phys. Lett. 78B, 217 (1978).
5. R. G. Lanier, L. G. Mann, G. L. Struble, I. D. Proctor, and D. W. Heikkinen, Phys. Rev. C 18, 1609 (1978).
6. R. G. Lanier, L. G. Mann, G. L. Struble, I. D. Proctor, and D. W. Heikkinen, Phys. Rev. C 20, 1279 (1979).
7. R. G. Lanier, G. L. Struble, L. G. Mann, I. C. Oelrich, I. D. Proctor, and D. W. Heikkinen, Phys. Rev. C 22, 51 (1980).
8. R. G. Lanier, G. L. Struble, L. G. Mann, W. Stöffl, I. C. Oelrich, J. Scheerer, I. D. Proctor, D. W. Heikkinen, and R. H. Howell, Phys. Lett. 99B, 23 (1981).
9. R. G. Lanier, R. K. Sheline, G. L. Struble, L. G. Mann, and J. A. Cizewski, Nucl. Phys. A413, 236 (1984).
10. B. C. Smith, Phys. Rev. C 19, 1107 (1979).
11. G. Løvholden, S. A. Hjorth, H. Ryde, and L. Harms-Ringdahl, Nucl. Phys. A181, 589 (1972).
12. G. Løvholden, J. C. Waddington, K. A. Hagemann, S. A. Hjorth, and H. Ryde, Nucl. Phys. A148, 657 (1970).

13. J. Kownacki, Z. Sujkowski, Z. Haratym, and H. Ryde, Proc. Int. Conf. on Reactions Between Complex Nuclei, Nashville, Tenn., 1, 174 (1974).
14. W. B. Cook, M. W. Johns, G. Løvholden, and J. C. Waddington, Nucl. Phys. A259, 461 (1976).
15. J. Rekstad, M. Guttormsen, T. Engeland, G. Løvholden, O. Straume, J. Lien, and C. E. Ellegaard, Nucl. Phys. A320, 239 (1979).
16. G. Løvholden and D. G. Burke, Can. J. Phys. 53 1182 (1975).
17. G. Løvholden, J. C. Waddington, C. Ellegaard, and P.O. Tjøm, Nucl. Phys. A160, 305 (1971).
18. D. E. Nelson, D. G. Burke, J. C. Waddington, and W. B. Cook, Can. J. Phys. 51, 2000 (1973).
19. M. Sekiguchi, Y. Shida, F. Soga, T. Hattori, Y. Hirao, and M. Sakai, Phys. Rev. Lett. 38, 1015 (1977).
20. R. J. Dupzyk, C. M. Henderson, W. M. Buckley, G. L. Struble, R. G. Lanier, and L. G. Mann, Nucl. Instr. and Meth. 102, 373 (1972).
21. E. R. Flynn, S. Orbesen, J. D. Sherman, J. W. Sunier, and R. Woods, Nucl. Instr. and Meth. 128, 35 (1975).
22. M. R. Schmorak, Nuclear Data Sheets 9, 195 (1973).
23. C. M. Lederer, Nuclear Data Sheets 35, 525 (1982).
24. R. D. Bagnell, Y. Tanaka, R. K. Sheline, D. G. Burke, and J. D. Sherman, Phys. Rev. C 20, 42 (1979).
25. W. Stöffl, Technical University, Munich, Germany (1980), computer code FITEK (private communication).
26. A. H. Wapstra and G. Audi, Nucl. Phys. A432 (1985).
27. The solid angles of the spectrograph and monitor counter, respectively, were measured as: $\Omega_S = 14.3 \times 10^{-3}$ sr and $\Omega_M = 8.659 \times 10^{-5}$ sr.

28. P. D. Kunz, Univ. of Colorado, Boulder, Colorado, computer code DWUCK
(private communication).
29. M. T. Lu and W. P. Alford, Phys. Rev. C 3, 1243 (1971).
30. A. H. Wapstra and K. Bos, Atomic Data and Nuclear Data Tables 19, 248-253
(1977).
31. B. E. Chi, Nucl. Phys. 83, 97 (1966).
32. Theoretical Nuclear Physics, Volume I: Nuclear Structure, A. E. de Shalit
and H. Feshbach, John Wiley & Sons, Inc., New York, N.Y. (1974), p. 417.
33. See for example "Single Nucleon Transfer in Deformed Nuclei" by B. Elbek
and P. O. Tjøm, pp. 259-323 in Advances in Nuclear Physics, Eds. M.
Baranger and E. Vogt, Plenum Press, New York, N.Y. (1960) or G. Løvnhøiden
and D. G. Burke, Can. J. Phys. 51, 2354 (1973).
34. Coupled-channel effects have been considered for deuteron projectiles with
several rare-earth targets by J. D. Peng, H. S. Song, F. C. Wang, and J.
V. Maher, Nucl. Phys. A341, 440 (1980).

TABLE 1

Nuclear levels in ^{151}Sm . The level energies are normalized to the 261.1-keV level in Ref. 14. Level energies in column 2 enclosed in parentheses indicate there is only weak evidence that the level is populated. Cross sections are quoted for the (t, α) reaction at $\theta_{\text{lab}} = 30^\circ$.

(t, α) group	Level Energy		I^π	Cross sections ($\mu\text{b/sr}$)
	(t, α) ^a (keV)	($\alpha, 3n\gamma$) ^b (keV)		
1	261	261.1	11/2 ⁻	18
2	447 ± 2	445.1	13/2 ⁻	16
3	651 ± 3	648.2	15/2 ⁻	2
4	870 ± 4	869.4	17/2 ⁻	<1
5	1167 ± 9			4
6	1271 ± 9			3
7	1398 ± 9			2
8	1489 ± 11			<1
9	1549 ± 10			2
10	(1636)			-
11	1697 ± 10			1
12	1747 ± 9			4
13	1771 ± 9			4
14	1815 ± 9			5
15	1845 ± 11			4
16	1871 ± 11			6
17	1894 ± 12			3
18	1953 ± 8			21
19	1991 ± 10			4
20	2045 ± 11			15
21	2080 ± 11			9
22	(2102)			-
23	(2119)			-
24	2134 ± 11			11
25	2165 ± 11			13
26	(2205)			-
27	2233 ± 13			5
28	2259 ± 13			4
29	2299 ± 11			11

^aQuoted errors are statistical only.

^bRef. 14.

TABLE 2

Nuclear levels in ^{153}Sm . The level energies are normalized to the 98.4-keV level in Ref. 15. Level energies in column 2 enclosed in parentheses indicate there is only weak evidence that the level is populated. Cross sections are quoted for the (t, α) reaction at $\theta_{\text{lab}} = 30^\circ$.

(t, α) group	Level Energy		I^π	Cross sections ($\mu\text{b/sr}$)
	(t, α) ^a (keV)	($\alpha, n\gamma$) ^b (keV)		
1	98	98.4	$11/2^-$	20
2	245 ± 2	245.8	$13/2^-$	18
3	411 ± 3	412.6	$15/2^-$	2
4	595 ± 5	597.5	$17/2^-$	-
5	1025 ± 10			2
6	(1089)			-
7	1130 ± 9			4
8	(1158)			-
9	(1201)			-
10	1254 ± 8			12
11	1299 ± 9			5
12	1336 ± 8			13
13	1368 ± 10			3
14	1404 ± 9			5
15	1439 ± 9			4
16	1486 ± 8			22
17	1516 ± 10			5
18	(1547)			-
19	1574 ± 9			6
20	1603 ± 10			5
21	1643 ± 11			8
22	1662 ± 12			7
23	1691 ± 10			6
24	1731 ± 12			4
25	1756 ± 8			17
26	1798 ± 8			13
27	(1833)			-
28	1847 ± 9			8
29	1875 ± 10			4
30	1914 ± 9			6
31	(1942)			-
32	1986 ± 11			8
33	2005 ± 12			10
34	2046 ± 11			8
35	2090 ± 11			9
36	2112 ± 14			5
37	2145 ± 12			10
38	2169 ± 13			5
39	2208 ± 11			11
40	2239 ± 12			6
41	(2390)			-

^aQuoted errors are statistical only.

^bRef. 15.

TABLE 3
Optical model parameters.²⁹

	t	α	p
$V_R(\text{MeV})$	200	200	(a)
$r_R(\text{fm})$	1.4	1.4	1.25
$a_R(\text{fm})$	0.6	0.6	0.65
$W(\text{MeV})$	50	20	-
$W_D(\text{MeV})$	-	-	-
$r_I(\text{fm})$	1.4	1.4	-
$a_I(\text{fm})$	0.6	0.6	-
$V_{so}(\text{MeV})$	-	-	$\lambda=10$
$r_c(\text{fm})$	1.3	1.3	1.25

^aAdjusted to give the correct separation energy.

TABLE 4

Calculated^a rotational parameters $\hbar^2/2I$ from (t, α) studies.

	¹⁵¹ Sm	¹⁵³ Sm
I_0	(keV)	(keV)
11/2	14.3	11.3
13/2	13.6	11.1
15/2	12.9	10.8

^aMoment of inertia parameters are determined from the energies of adjacent spin levels through the relationship:

$$\Delta E = \hbar^2/2I \cdot 2[I_0 + 1],$$

where I_0 is the lower spin.

TABLE 5

Spectroscopic amplitudes. The terms given below assume a two-quasiparticle initial state given by $K_A > = \Omega_\alpha \tilde{\Omega}_\beta >$, where $K_A = \Omega_\alpha - \Omega_\beta$, and a final one- or three-quasiparticle state $K_B >$. One-quasiparticle final states are formed by pickup of one of the valance particles (Ω_α or Ω_β), while three-quasiparticle states are formed by leaving the valance particles coupled to K_A and picking up a nucleon, Ω_γ , from a spin-zero coupled pair.

<u>Final State</u>		<u>Spectroscopic Amplitude^a</u>
$\chi_{K_B} >$	K_B	$A_{lsj} / \frac{2I_A + 1}{2I_B + 1}$
$\Omega_\alpha >$	Ω_α	$\langle I_A K_A j \Omega_\beta \ I_B K_B \rangle U_\beta W_{lj\Omega_\beta}^\beta$
$\Omega_\beta >$	Ω_β	$(-)^{I_A + M_A} \langle I_A - K_A j \Omega_\alpha \ I_B K_B \rangle U_\alpha W_{lj\Omega_\alpha}^\alpha$
$\Omega_\alpha \tilde{\Omega}_\beta \Omega_\gamma >$	$K_A + \Omega_\gamma$	$\langle I_A K_A j \Omega_\gamma \ I_B K_B \rangle V_\gamma W_{lj\Omega_\gamma}^\gamma$
$\Omega_\alpha \tilde{\Omega}_\beta \tilde{\Omega}_\gamma >$	$K_A - \Omega_\gamma$	$(-)^{j + \Omega_\gamma} \langle I_A K_A j - \Omega_\gamma \ I_B K_B \rangle V_\gamma W_{lj\Omega_\gamma}^\gamma$

^a $I_{A,B}$, the total spin of the initial and final states, respectively;
 $K_{A,B}$, the projection of $I_{A,B}$ on the nuclear symmetry axis; j , the total spin of the transferred nucleon; Ω , the projection of j on the nuclear symmetry axis; V, U are occupation probabilities, and W are the Nilsson amplitudes.

TABLE 6

Angle-integrated cross sections.

Experimental integrated ^a cross sections			
I	¹⁵¹ Sm (μ b)	¹⁵³ Sm (μ b)	Ratio (151/153)
11/2	17 \pm 3	22 \pm 2	0.77 \pm 0.15
13/2	15 \pm 3	19 \pm 2	0.79 \pm 0.18
Theoretical integrated ^a cross sections			
I	¹⁵¹ Sm (μ b)	¹⁵³ Sm (μ b)	Ratio (151/153)
11/2	15	15	1.0
13/2	16	16	1.0

^aThe angle-integrated cross sections were calculated with the angular limits of integration from 12.5° to 30° by the relation:

$$\sigma_T = 2\pi \int_1 \frac{d\sigma}{d\Omega}(\theta_1) \cdot \sin \theta_1 \cdot \Delta\theta_1.$$

FIGURE CAPTIONS

- FIG. 1 Alpha particle spectrum from the $^{152}\text{Eu}(t,\alpha)$ reaction at 30° . The peaks belonging to ^{151}Sm are labeled to correspond with the numbering in Table 1. The expected position of any ground state (G.S.) population is noted. Regions of the spectrum labeled A and B are discussed in the text.
- FIG. 2 Alpha particle spectrum from the $^{154}\text{Eu}(t,\alpha)$ reaction at 30° . The inset shows relevant data obtained at 50° . The peaks belonging to ^{153}Sm are labeled to correspond with the numbering in Table 2. See caption, Fig. 1.
- FIG. 3 Angular distributions for the first three states observed in the $^{152}\text{Eu}(t,\alpha)$ reaction. The data points with error bars are absolute experimental differential cross sections and the solid curves are unadjusted theoretical values.
- FIG. 4 Angular distributions for the first three states observed in the $^{154}\text{Eu}(t,\alpha)$ reaction. See caption, Fig. 3.
- FIG. 5 Binding energy of the last two neutrons, S_{2n} , as a function of the mass number, A , for the rare-earth transitional isotopes Dy, Gd, Sm, and Nd. Error bars are given only when larger than the plotted data point; labeled heavy solid lines are drawn through the points to show the general trend in each nucleus, and the numbered light lines are drawn to connect isotonic points.
- FIG. 6 Comparison of the experimental and calculated (t,α) intensities in ^{151}Sm and ^{153}Sm at 30° for the $11/2[505]$ band.

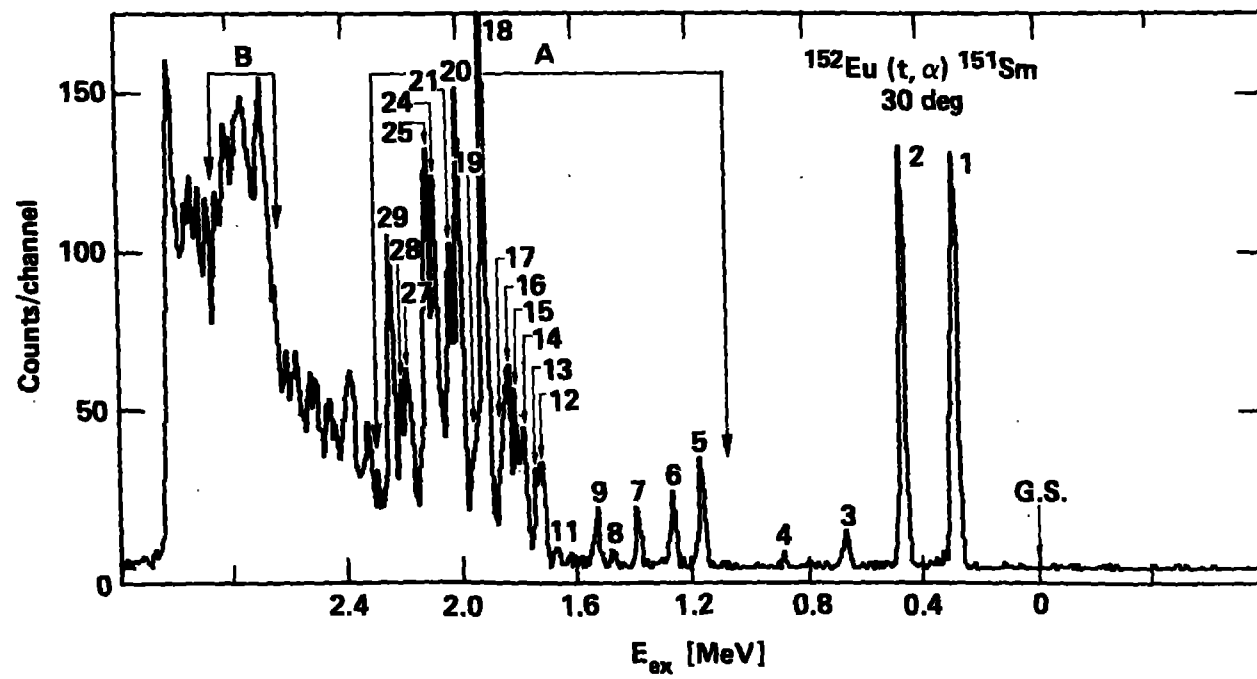


Fig. 1

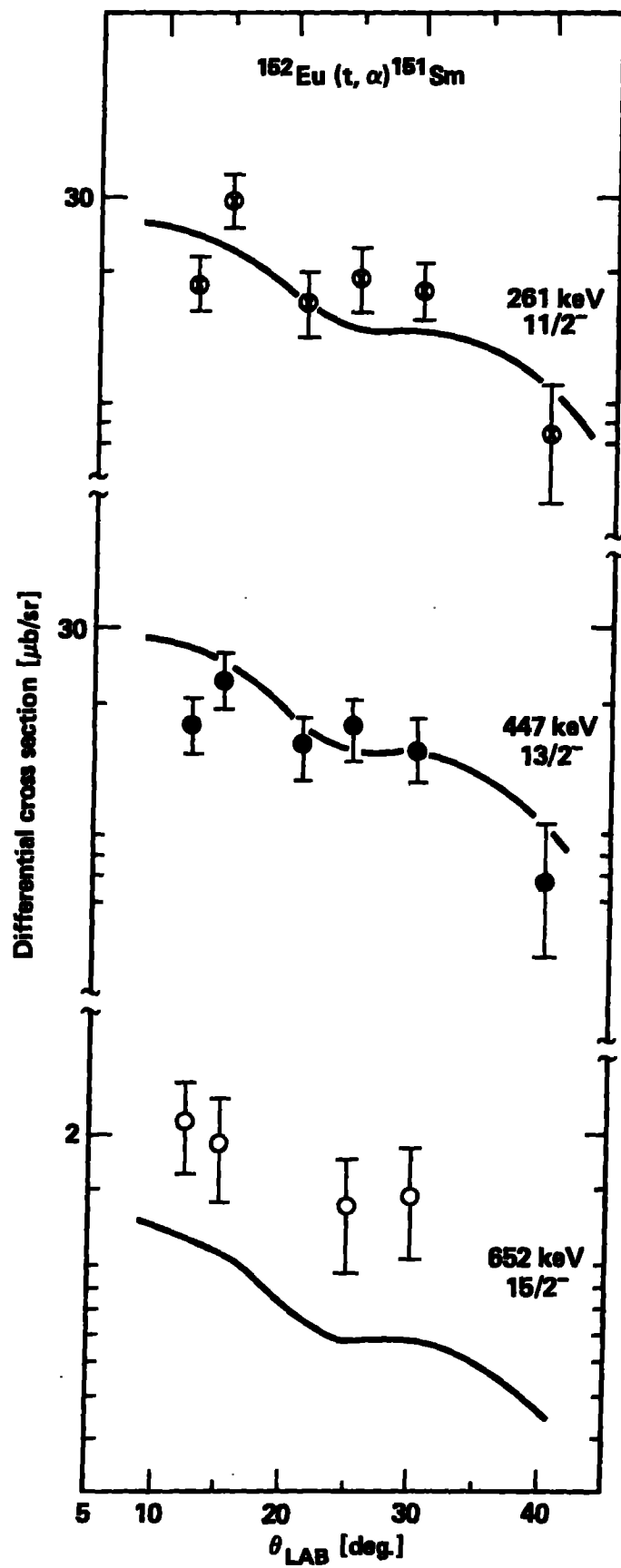


Fig. 3

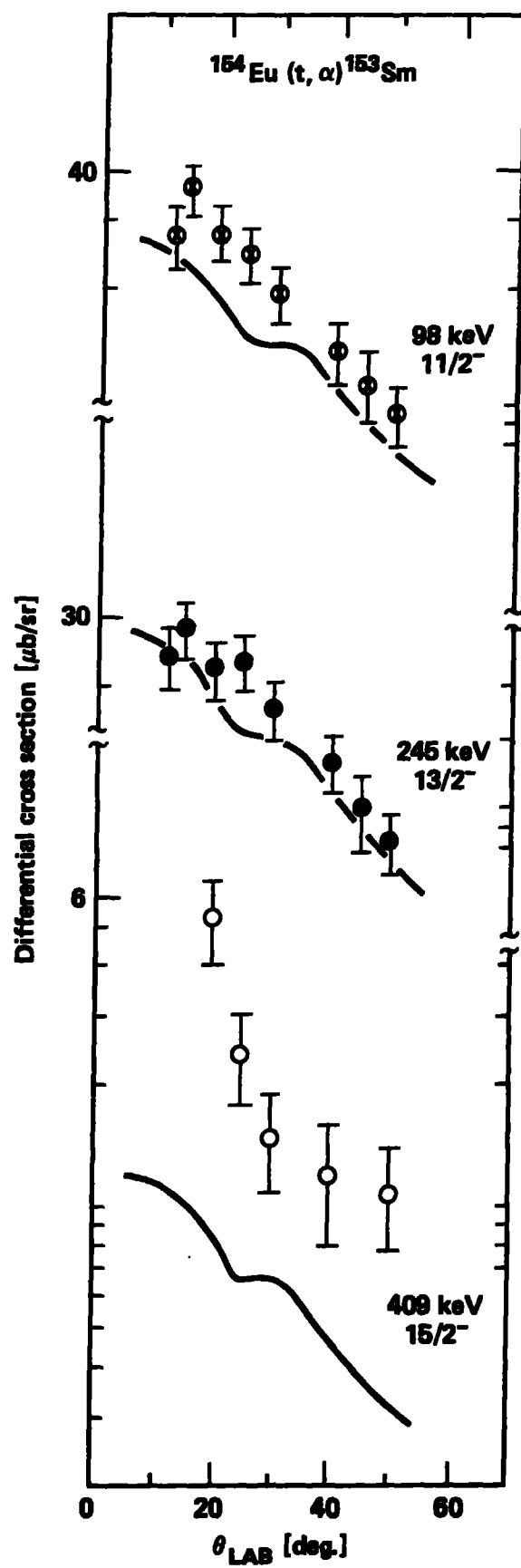


Fig. 4

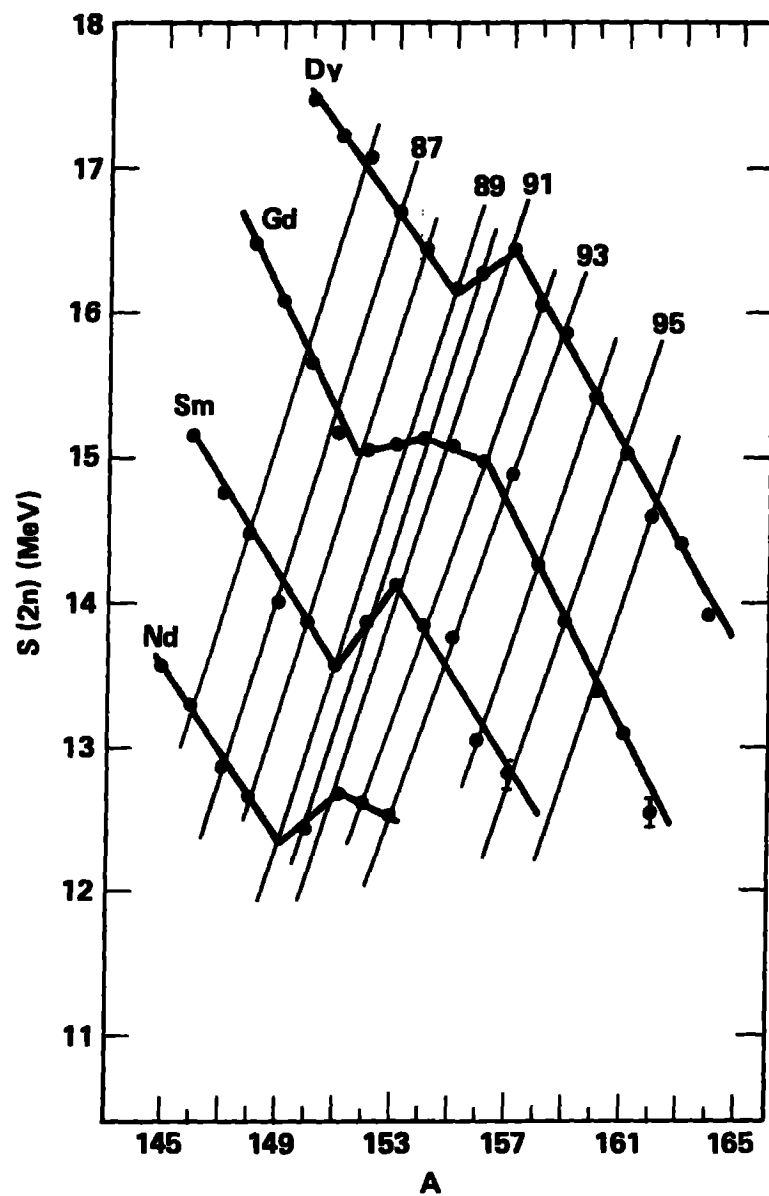


Fig. 5

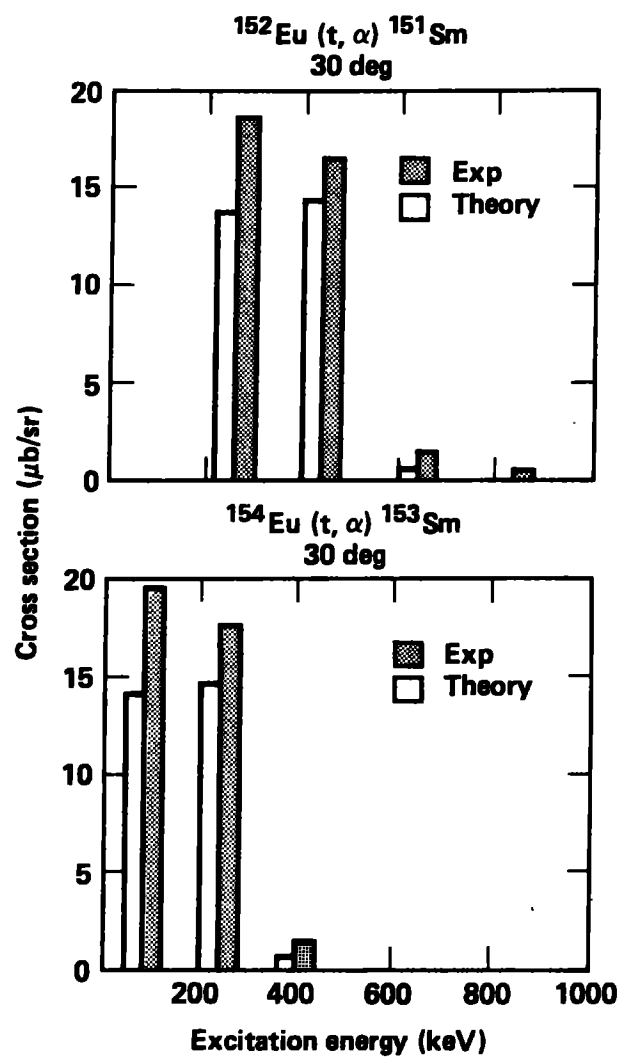


Fig. 6